NASA TECHNICAL NOTE

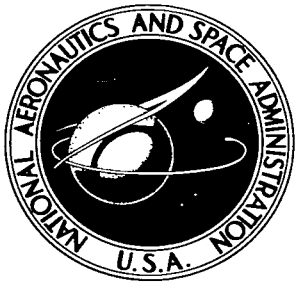

NASA TN D-4133
c.1

NASA TN D-4133

THF EFFECT OF PLANETARY ALBEDO ON SOLAR ORIENTATION OF SPACECRAFT

by Anthony Fontana

Langley Research Center
Langley Station, Hampton, Va.

NATIONAL AERONAUTICS AND SPACE ADMINISTRATION • WASHINGTON, D. C. • SEPTEMBER 1967

NASA TN D-4133

THE EFFECT OF PLANETARY ALBEDO ON SOLAR ORIENTATION OF SPACECRAFT

By Anthony Fontana

Langley Research Center
Langley Station, Hampton, Va.

NATIONAL AERONAUTICS AND SPACE ADMINISTRATION

For sale by the Clearinghouse for Federal Scientific and Technical Information
Springfield, Virginia 22151 – CFSTI price $3.00

THE EFFECT OF PLANETARY ALBEDO ON SOLAR ORIENTATION OF SPACECRAFT

By Anthony Fontana
Langley Research Center

SUMMARY

The analytical expression for the solar orientation error caused by planetary albedo is derived. A typical solar sensor output characteristic is assumed and a computer solution to the analytical expression is obtained. The computer results are presented for a spacecraft in the vicinity of Earth, Venus, Mars, and the Moon. Each planetary body is assumed to be a spherical diffuse reflector with cylindrical shadows and a constant albedo. The data generated herein permit the selection of an appropriate coarse-sensor to fine-sensor switching angle for solar orientation control systems and facilitate the interpretation of solar-referenced scientific experiment data.

INTRODUCTION

A variety of space missions require solar orientation of the spacecraft for scientific observation and study of the Sun, solar power conversion, temperature balance, navigational reference, data interpretation, and so forth. Generally, solar orientation is achieved through the use of solar radiation sensors and an attitude control system. Solar orientation may become inaccurate when the spacecraft is in the vicinity of a planetary body, because the solar sensors receive both direct solar radiation and solar radiation reflected from the planet. These inaccuracies may be eliminated through the use of coarse and fine solar sensors. Typically, coarse sensors have a spherical field of view and thus see both sources of radiation, the Sun and the planet. The attitude control system, while operating on the coarse-sensor signals, orientates the spacecraft toward a point located between the two radiation sources. The resulting orientation error is dependent on the relative intensities of the radiation sources and their angular separation. Typically, the fine sensors have a restricted field of view and under favorable conditions see only one of the two sources of radiation.

The logic of coarse/fine solar sensing is discussed in reference 1 and is explained briefly as follows. The coarse sensors are used during Sun capture maneuvers. At a predetermined angular pointing error, control of the spacecraft is switched from the coarse sensors to the fine sensors. Once the fine sensors are activated, orientation

error is not introduced by planetary albedo, except during the fraction of the orbit or trajectory when the angular separation between the Sun and the planet is less than the field of view of the fine sensors – that is, when the Sun is near the planet horizon. The successful use of this logic is predicated on a prior knowledge of the magnitude of the orientation error which can be introduced by the albedo of a planet. It should be noted that the coarse-sensor to fine-sensor switching angle (angular pointing error at which control is switched from the coarse sensors to the fine sensors) must be greater than the maximum orientation error. The purpose of this paper is to generate the data required for selection of the proper coarse-sensor to fine-sensor switching angle for solar-orientated spacecraft.

The problem to be solved is essentially one of calculating the radiation balance between two coarse solar sensors (a pitchup sensor and a pitchdown sensor) and therefore is related to the calculation of the thermal balance of a spacecraft. The investigation of the thermal balance of an arbitrarily orientated flat plate is particularly applicable to the problem at hand. In references 2 and 3 the total thermal balance of a flat plate is considered, and in reference 4 the albedo radiation incident upon an arbitrarily orientated spinning flat plate is calculated. In the present paper the concepts and equations generated in the preceding thermal-balance studies have been modified and applied to the solar orientation problem. The solar orientation error introduced by planetary albedo is calculated for a spacecraft in the vicinity of Earth, Venus, Mars, and the Moon.

SYMBOLS

a planetary albedo (fraction of solar radiation reflected by planetary body)

C constant, $\frac{2aR^2}{\pi}$, kilometers^2

ds element of planetary surface area, meters^2

D distance between ds and solar sensor, kilometers

$F(\theta,\phi,\epsilon,\psi,H)$ integrand of general error equation (eq. (11)), degrees

h altitude of solar sensor, kilometers

H solar-sensor altitude plus planetary radius, kilometers

K solar constant, watts/meter^2

R	planetary radius, kilometers
X,Y,Z	orthogonal reference system defined by local vertical (Z-axis) and plane formed by centers of planet, Sun, and spacecraft (YZ-plane)
β	angle between solar vector and normal to ds, degrees
γ	angle between normal to ds and ds-sensor line, degrees
δ	angle between Z-axis and ds-sensor line, degrees
ϵ	solar orientation error, degrees
ϵ_{max}	maximum orientation error at given altitude, degrees
θ	colatitudinal coordinate of ds, degrees
θ_m	angle between Z-axis and perpendicular line connecting planet center to tangent from sensor to planet surface, degrees
θ_1	angle between Z-axis and line connecting planet center to point of intersection of extended sensor plane with planet surface in YZ-plane, degrees
λ	angle between sensor plane and ds-sensor line, degrees
ξ	angle between normal to sensor plane and ds-sensor line, degrees
σ	angle between Z-axis and normal to sensor plane, degrees
ϕ	longitudinal coordinate of ds, degrees
ψ	angle between Z-axis and solar vector (planetocentric angle, in general, with subscripts Earth, Venus, Mars, and Moon denoting, in particular, geocentric, aphrodiocentric, areocentric, and lunicentric angles, respectively)

ASSUMPTIONS

Direct Solar Radiation

The equations which describe the problem are set up in terms of radiation balance. Therefore, the solar constant can be set equal to unity at any given location of the spacecraft in the solar system.

The Sun is assumed to be located at infinity relative to the spacecraft. Planet shadows are, therefore, assumed cylindrical, and penumbral effects are ignored. This assumption simplifies the calculations and introduces negligible error.

Albedo Radiation

The mean albedos and mean radii of various planetary bodies (from ref. 5) are as follows:

	Mean albedo	Mean radius
Earth	0.39	6367.5 km
Venus	0.76	6100 km
Mars	0.16	3377 km
Moon	0.07	1738 km

The albedos of Venus, Mars, and the Moon are relatively constant over the surface of the bodies due to the absence of polar caps and/or extremes in atmospheric density. However, the albedo of Earth varies with latitude and season of the year due to variable cloud, vegetation, water, and snow cover. The Tiros VII meteorological satellite monitored the Earth albedo, in the 0.55- to 0.75-micron band with a 5^{o} field-of-view sensor, from June 1963 to May 1964 (ref. 6). The albedo varied from a minimum of approximately 0.15 to a maximum of approximately 0.70. The mean albedo for the 1-year period was 0.32. The Tiros VII data are in general agreement with the values of albedo deduced from the emissivity sensors of the first Orbiting Solar Observatory (ref. 7) and the albedo values calculated in reference 8; however, the variations in the Earth albedo are not sufficiently defined to warrant detailed consideration. In this paper the solar orientation error is calculated for two values of constant Earth albedo. An Earth albedo of 0.35 is used to calculate the nominal orientation error, and an Earth albedo of 0.50 is used to calculate the worst expected orientation error. (Although Tiros VII measured albedos in excess of 0.50 with a 5^{o} field-of-view sensor, the averaging effect of the large field of view of the coarse solar sensors reduces the worst expected albedo to approximately 0.50.)

All planetary bodies are assumed to be spherical. The spectral distribution of albedo radiation is assumed to be identical to the spectral distribution of direct solar radiation. All planetary bodies are assumed to be diffuse reflectors – that is, Lambert's cosine law is obeyed.

Solar Sensors

The solar sensors are assumed to be of the null type with a sinusoidal output characteristic as shown in figure 1. The sinusoidal output characteristic closely approximates the output characteristic presented in reference 9 (for coarse sensors of the type used on the Orbiting Solar Observatory, the Orbiting Astronomical Observatory, the Orbiting Geophysical Observatory, and Lunar Orbiter) and the coarse-sensor output characteristic of two silicon solar cells mounted back-to-back (ref. 1). The latter coarse-sensor characteristic is shown in figure 1 for comparison with the sinusoidal approximation.

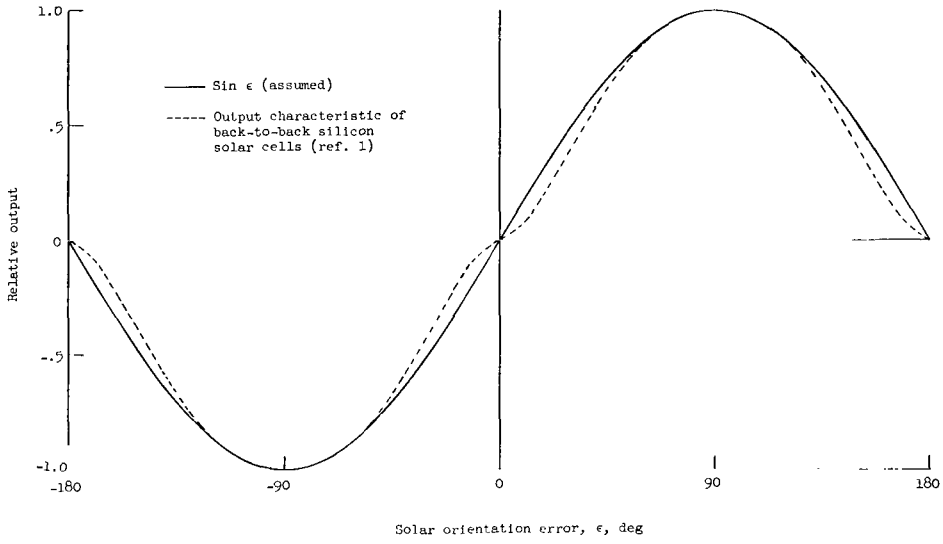

Figure 1.- Comparison of assumed and actual solar sensor output characteristics.

The pitch plane of the spacecraft is assumed to coincide with the plane defined by the centers of the planet, spacecraft, and Sun (the YZ-plane). By restricting the orientation of the pitch plane, all orientation errors are forced to occur in the pitch plane because of yaw-plane symmetry. The preceding assumption simplifies the calculations without affecting accuracy (i.e., accuracy is not affected if the pitch and yaw solar sensors are calibrated such that the absolute value of the vector sum of the pitch-axis and yaw-axis pointing errors remains constant as the spacecraft is rolled about a fixed roll-axis orientation).

ANALYTICAL TREATMENT

The problem geometry is illustrated in figure 2. For the purpose of problem visualization, consider pitch-plane coarse sensors composed of two silicon solar cells mounted

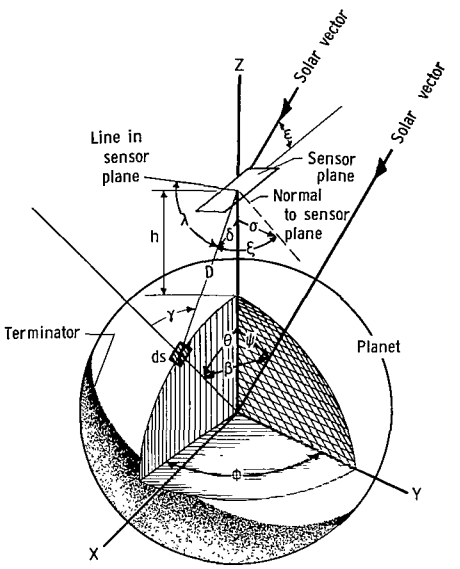

Figure 2.- Problem geometry.

back-to-back and having a sinusoidal output characteristic. The plane of the silicon solar cells is referred to as the sensor plane. (The sensor plane is always perpendicular to the YZ-plane by a previous assumption.)

The attitude control system maneuvers the spacecraft until the output of the solar sensors is zero – that is, until a balance exists between the radiation incident on the pitchup coarse sensor and the radiation incident on the pitchdown coarse sensor. The general expression for the radiation balance is

$$\frac{Ka}{\pi}\int \frac{\cos\beta\cos\gamma\sin\lambda}{D^2}\,ds - K\sin\epsilon = 0 \qquad (1)$$

where the first term describes the albedo radiation and the second term describes the direct solar radiation. In equation (1), $K\cos\beta\,ds$ is the solar irradiance incident on ds (see fig. 2) and $\frac{Ka\cos\beta\,ds}{\pi}$ is the solar radiance reflected by ds. The latter quantity multiplied by $\cos\gamma$ gives the radiance reflected from ds in the direction of the spacecraft (by Lambert's cosine law for diffuse reflection). Division by D^2 gives the irradiance of the albedo at the spacecraft. Both $\sin\lambda$ and $\sin\epsilon$ are weighting functions of the assumed solar sensor output characteristic (fig. 1).

The following relations are obtained from the geometry of figure 2:

$$H = h + R \qquad (2)$$

$$ds = R^2\sin\theta\,d\theta\,d\phi \qquad (3)$$

$$D^2 = H^2 + R^2 - 2RH\cos\theta \qquad (4)$$

$$\cos\gamma = \frac{H\cos\theta - R}{D} \qquad (5)$$

$$\cos \beta = \cos \theta \cos \psi + \sin \theta \sin \psi \cos \phi \tag{6}$$

$$\sin \lambda = \cos \xi = \cos \delta \cos \sigma + \sin \delta \sin \sigma \cos \phi \tag{7}$$

$$\sin \delta = \frac{R \sin \theta}{D} \tag{8}$$

$$\cos \delta = \frac{H - R \cos \theta}{D} \tag{9}$$

$$\sigma = \left| \frac{\pi}{2} - \psi - \epsilon \right| \tag{10}$$

Division of equation (1) by K and substitution of the preceding relations yield

$$\frac{2aR^2}{\pi} \int_0^{\theta} \int_0^{\phi} (\cos \theta \cos \psi + \sin \theta \sin \psi \cos \phi)(H \cos \theta - R)\left[(H - R \cos \theta)\left(\cos\left|\frac{\pi}{2} - \psi - \epsilon\right|\right) + R \sin \theta \left(\sin\left|\frac{\pi}{2} - \psi - \epsilon\right|\right) \cos \phi\right] \sin \theta \, d\phi \, d\theta \Big/ \left(H^2 + R^2 - 2RH \cos \theta\right)^2 - \sin \epsilon = 0 \tag{11}$$

By letting C equal $\frac{2aR^2}{\pi}$ and letting $\int_0^{\theta} \int_0^{\phi} F(\theta, \phi, \epsilon, \psi, H) d\phi \, d\theta$ represent the integral in equation (11), equation (11) may be written in simplified notation as

$$C \int_0^{\theta} \int_0^{\phi} F(\theta, \phi, \epsilon, \psi, H) d\phi \, d\theta - \sin \epsilon = 0 \tag{12}$$

The computer solution of equation (12) requires iteration on ϵ and numerical integration with respect to ϕ and θ. The limits of integration depend on the problem geometry; the various geometrical cases which can occur are outlined as follows. It should be noted that the conditions for occurrence of each geometrical case define the logical flow of information within the computer program and must be satisfied in the order given.

I. Sensors see totally sunlit area.

A. Sensor plane does not cut sunlit area (fig. 3).

1. Conditions for occurrence

a. $\psi < \frac{\pi}{2}$

b. $\theta_m \leqq \frac{\pi}{2} - \psi$

c. $\epsilon \geqq \frac{\pi}{2} - \psi - \theta_m$

2. Equation (12) becomes

$$C\int_0^{\theta_m}\int_0^{\pi} F(\theta,\phi,\epsilon,\psi,H)d\phi\ d\theta = \sin\epsilon \tag{13}$$

where

$$\theta_m = \cos^{-1}\frac{R}{H} \tag{14}$$

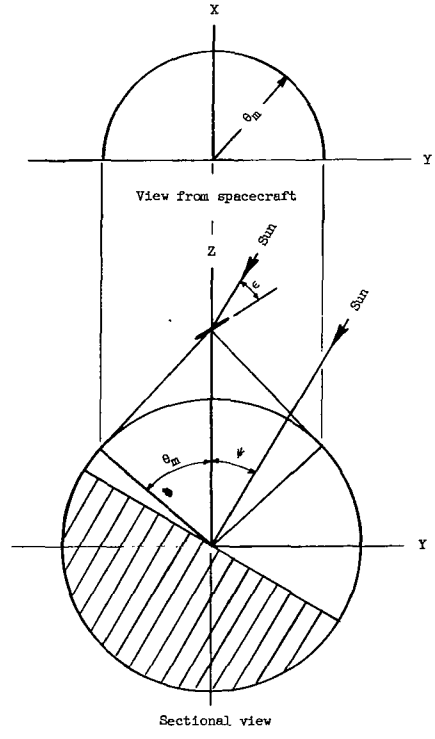

Figure 3.- Geometry for case I-A.

B. Sensor plane cuts sunlit area (fig. 4).

1. Conditions for occurrence

   a. $\psi < \frac{\pi}{2}$

   b. $\theta_m \leqq \frac{\pi}{2} - \psi$

   c. $\epsilon < \frac{\pi}{2} - \psi - \theta_m$

2. Equation (12) becomes

$$C\int_0^{\theta_1}\int_0^{\pi} F(\theta,\phi,\epsilon,\psi,H)\,d\phi\,d\theta + C\int_{\theta_1}^{\theta_m}\int_0^{\frac{\pi}{2}+\sin^{-1}\left(\frac{H-R\cos\theta}{R\sin\theta\tan\left|\frac{\pi}{2}-\psi-\epsilon\right|}\right)} F(\theta,\phi,\epsilon,\psi,H)\,d\phi\,d\theta - C\int_{\theta_1}^{\theta_m}\int_{\frac{\pi}{2}+\sin^{-1}\left(\frac{H-R\cos\theta}{R\sin\theta\tan\left|\frac{\pi}{2}-\psi-\epsilon\right|}\right)}^{\pi} F(\theta,\phi,\epsilon,\psi,H)\,d\phi\,d\theta = \sin\epsilon \qquad (15)$$

where

$$\theta_m = \cos^{-1}\frac{R}{H}; \qquad \theta_1 = \sin^{-1}\left[\frac{H}{R}\sin(\psi+\epsilon)\right] - (\psi+\epsilon) \qquad (16)$$

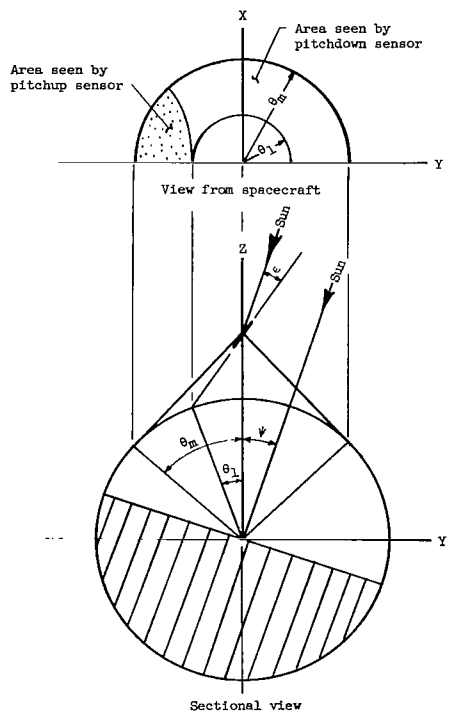

Figure 4.- Geometry for case I-B.

II. Sensors do not see totally sunlit area.

A. Sensor plane does not cut sunlit area.

1. Figure 5

a. Conditions for occurrence

(1) $\psi < \frac{\pi}{2}$

(2) $\theta_m > \frac{\pi}{2} - \psi$

(3) $\epsilon \leq \frac{\pi}{2} - \psi + \theta_m$

b. Equation (12) becomes

$$C \int_0^{\frac{\pi}{2}-\psi} \int_0^{\pi} F(\theta,\phi,\epsilon,\psi,H)d\phi \; d\theta$$

$$+ C \int_{\frac{\pi}{2}-\psi}^{\theta_m} \int_0^{\frac{\pi}{2}+\sin^{-1}(\cot\psi \cot\theta)} F(\theta,\phi,\epsilon,\psi,H)d\phi \; d\theta = \sin\epsilon \qquad (17)$$

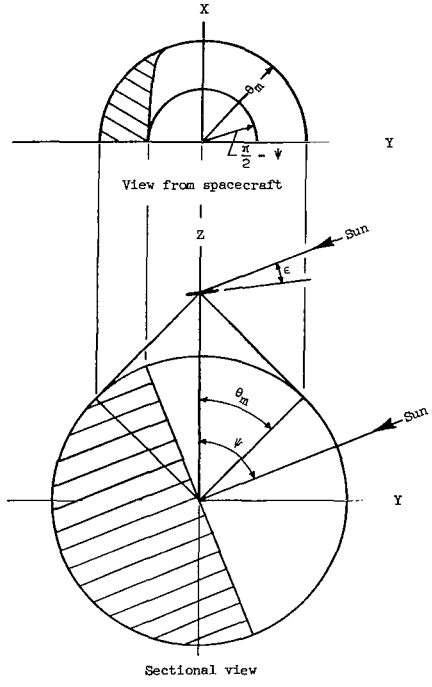

Figure 5.- Geometry for case II-A-1.

2. Figure 6

a. Conditions for occurrence

(1) $\frac{\pi}{2} \leqq \psi \leqq \frac{\pi}{2} + \theta_m$

(2) $\theta_m > \psi - \frac{\pi}{2}$

(3) $\epsilon \leqq \frac{\pi}{2} - \psi + \theta_m$

b. Equation (12) becomes

$$C \int_{\psi - \frac{\pi}{2}}^{\theta_m} \int_{0}^{\frac{\pi}{2} + \sin^{-1}(\cot\psi \cot\theta)} F(\theta, \phi, \epsilon, \psi, H) d\phi \; d\theta = \sin \epsilon \qquad (18)$$

Note: If $\psi > \frac{\pi}{2} + \theta_m$, the sensors see a totally dark area and no error results.

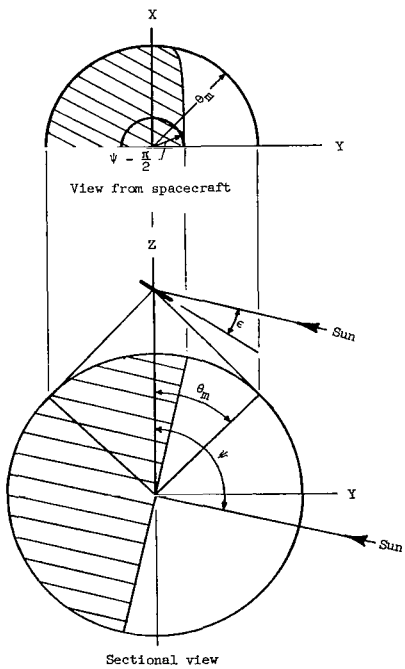

Figure 6.- Geometry for case II-A-2.

B. Sensor plane cuts sunlit area.

1. Figure 7

a. Conditions for occurrence:

(1) $\psi < \frac{\pi}{2}$

(2) $\theta_m > \frac{\pi}{2} - \psi$

(3) $\epsilon > \frac{\pi}{2} - \psi + \theta_m$

b. Equation (12) becomes

$$C\int_0^{\frac{\pi}{2}-\psi}\int_0^{\pi} F(\theta,\phi,\epsilon,\psi,H)\,d\phi\,d\theta + C\int_{\frac{\pi}{2}-\psi}^{\theta_1}\int_0^{\frac{\pi}{2}+\sin^{-1}(\cot\psi\cot\theta)} F(\theta,\phi,\epsilon,\psi,H)\,d\phi\,d\theta$$

$$+ C\int_{\theta_1}^{\theta_m}\int_{\frac{\pi}{2}-\sin^{-1}\left(\frac{H-R\cos\theta}{R\sin\theta\tan\left|\frac{\pi}{2}-\psi-\epsilon\right|}\right)}^{\frac{\pi}{2}+\sin^{-1}(\cot\psi\cot\theta)} F(\theta,\phi,\epsilon,\psi,H)\,d\phi\,d\theta - C\int_{\theta_1}^{\theta_m}\int_0^{\frac{\pi}{2}-\sin^{-1}\left(\frac{H-R\cos\theta}{R\sin\theta\tan\left|\frac{\pi}{2}-\psi-\epsilon\right|}\right)} F(\theta,\phi,\epsilon,\psi,H)\,d\phi\,d\theta = \sin\epsilon \qquad (19)$$

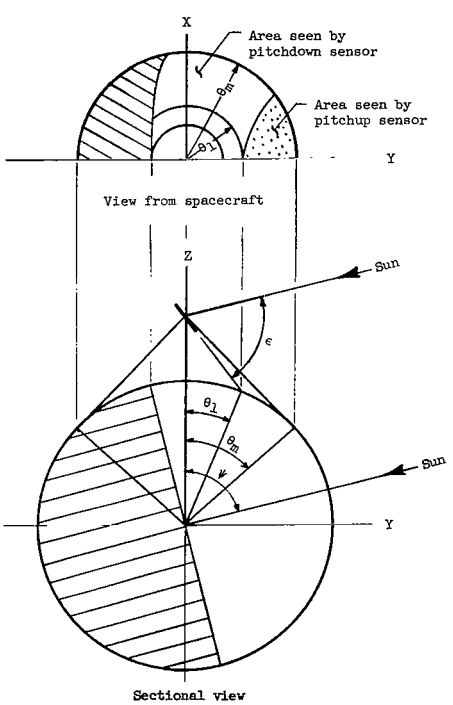

Figure 7.- Geometry for case II-B-1.

2. Figure 8

a. Conditions for occurrence:

(1) $\frac{\pi}{2} \leqq \psi \leqq \frac{\pi}{2} + \theta_m$

(2) $\theta_m > \psi - \frac{\pi}{2}$

(3) $\epsilon > \frac{\pi}{2} - \psi + \theta_m$

b. Equation (12) becomes

$$C \int_{\psi - \frac{\pi}{2}}^{\theta_1} \int_{0}^{\frac{\pi}{2} + \sin^{-1}(\cot\psi \cot\theta)} F(\theta,\phi,\epsilon,\psi,H)\,d\phi\,d\theta + C \int_{\theta_1}^{\theta_m} \int_{\frac{\pi}{2} - \sin^{-1}\left(\frac{H - R\cos\theta}{R\sin\theta\tan\left|\frac{\pi}{2} - \psi - \epsilon\right|}\right)}^{\frac{\pi}{2} + \sin^{-1}(\cot\psi\cot\theta)} F(\theta,\phi,\epsilon,\psi,H)\,d\phi\,d\theta$$

$$- C \int_{\theta_1}^{\theta_m} \int_{0}^{\frac{\pi}{2} - \sin^{-1}\left(\frac{H - R\cos\theta}{R\sin\theta\tan\left|\frac{\pi}{2} - \psi - \epsilon\right|}\right)} F(\theta,\phi,\epsilon,\psi,H)\,d\phi\,d\theta = \sin\epsilon \qquad (20)$$

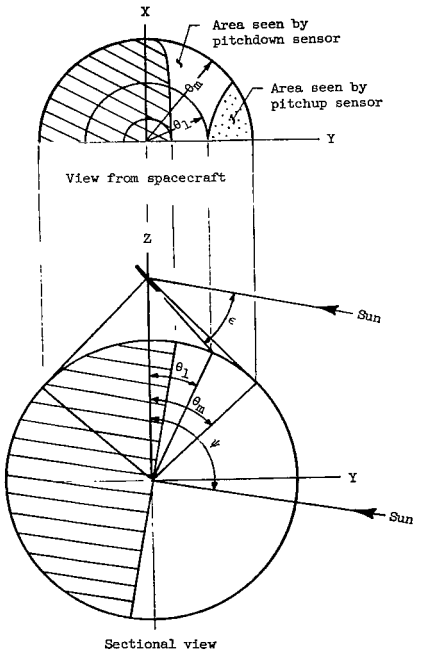

Figure 8.- Geometry for case II-B-2.

RESULTS AND DISCUSSION

The computer solutions of equation (11) are presented in tables I to V. The orientation error ϵ is tabulated for selected values of planetocentric angle ψ and altitude h. Table I presents the nominal orientation error due to the Earth albedo (a = 0.35), and table II presents the worst expected orientation error due to the Earth albedo (a = 0.50). Tables III, IV, and V present the orientation error due to the Venus, Mars, and Moon albedos, respectively. The low densities of the Mars and Moon atmospheres allow relatively low orbital altitudes; therefore, the minimum altitude was reduced from 100 kilometers to 50 kilometers in the computer programs for Mars and the Moon. In each table the orientation errors (even if zero) are indicated until the planetocentric angle is greater than $\frac{\pi}{2} + \theta_m$ – that is, until the solar sensors see a totally dark planetary body. In order to remain commensurate with the accuracy of the analytic expressions, the computer was instructed to satisfy equation (11) only to the nearest 0.1°; therefore, the tabulated computer results have been rounded off to a single decimal.

The solar orientation errors calculated herein are the vector sum of the pitch and yaw errors. In this investigation the roll attitude of the spacecraft was fixed so that the errors would lie in the pitch plane exclusively (see "Assumptions" section). When the pitch plane does not coincide with the YZ-plane (see fig. 2), the individual pitch and yaw

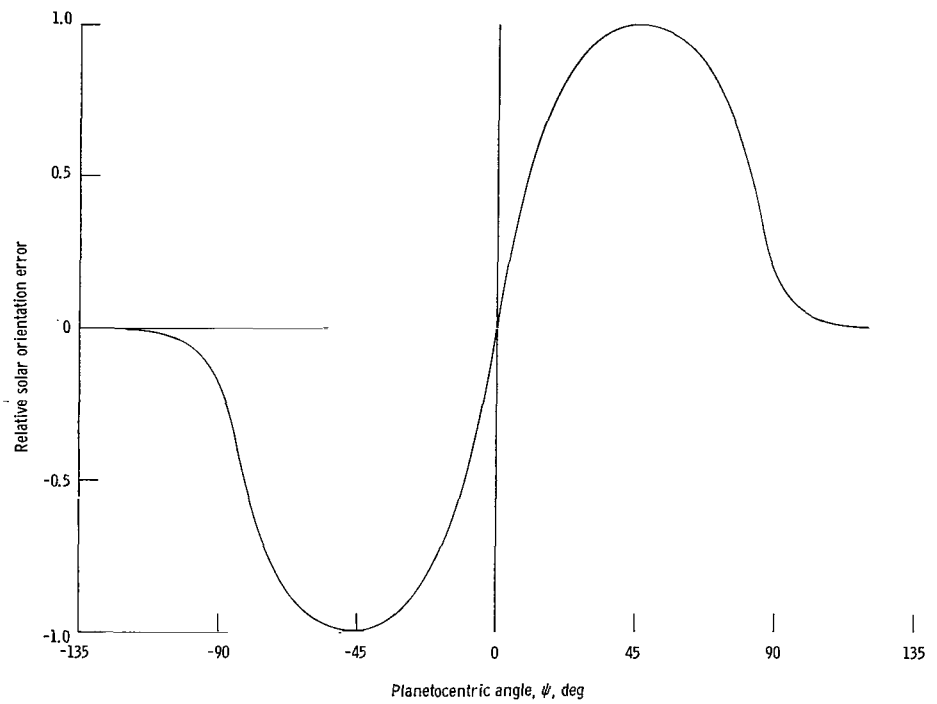

Figure 9.- Typical variation of solar orientation error with planetocentric angle.

errors can be determined by resolving the tabulated resultant error into pitch and yaw components.

The shape of the general relation between the solar orientation error ϵ and the planetocentric angle ψ is illustrated in figure 9. Symmetry about the ordinate results from the assumption of a constant albedo. Selected data from tables I to V are presented graphically in figures 10 to 14. The maximum orientation error occurs between the planetocentric angles of 30^{o} and 45^{o}. The tapering off of the curves beyond $\psi = 90^{o}$ occurs as the Sun approaches the planet horizon and is caused, primarily, by the gradual decrease in the angular size of the illuminated limb of the planetary body.

In figure 15 the maximum orientation error for a given altitude ϵ_{max} is plotted as a function of altitude. Curves are shown for the various planetary bodies under consideration. As expected (from inspection of the analytic expressions), the solar orientation error increases with increasing albedo and decreases with increasing altitude. Since the radius of Venus is approximately equal to the radius of Earth, the solar orientation error caused by the Venus albedo is representative of the error that would result from an Earth albedo of 0.76. An Earth albedo of approximately 0.76 is appropriate for a worst-case analysis.

The data generated in this paper can be used to specify the solar pointing error at which control of the spacecraft should be switched from the coarse solar sensors to the fine solar sensors. For example, consider a spacecraft in an Earth orbit with a perigee of 500 kilometers. Capture of the solar target, from a large initial pointing error, can be attained only if the coarse-sensor to fine-sensor switching angle is greater than the maximum solar orientation error. As shown in figure 11, the maximum orientation error occurs when perigee coincides with a geocentric angle of 36^{o}; the value of the error is 16.4^{o}. Therefore, for a spacecraft in an Earth orbit with a perigee of 500 kilometers, the coarse-sensor to fine-sensor switching angle must be greater than 16.4^{o}. The actual switching angle would be equal to 16.4^{o} plus an appropriate safety factor. The magnitude of the safety factor depends on how well the actual coarse-sensor output characteristic matches the assumed sinusoidal coarse-sensor output characteristic (fig. 1) and should be as small as possible to avoid unnecessary increases in the fine-sensor field of view.

The data generated in this paper are also applicable to spacecraft which are equipped with only one set of solar sensors – that is, coarse sensors only. Assume that a single set of coarse solar sensors are used to orient a spacecraft toward the Sun. Further assume that the spacecraft is equipped with various instruments and experiments which depend on the solar reference for correct data interpretation. If the orbital elements of the spacecraft and the celestial position of the Sun are known, the planetocentric angle can be calculated and the appropriate table used to determine the orientation of the onboard instruments and experiments relative to the solar reference.

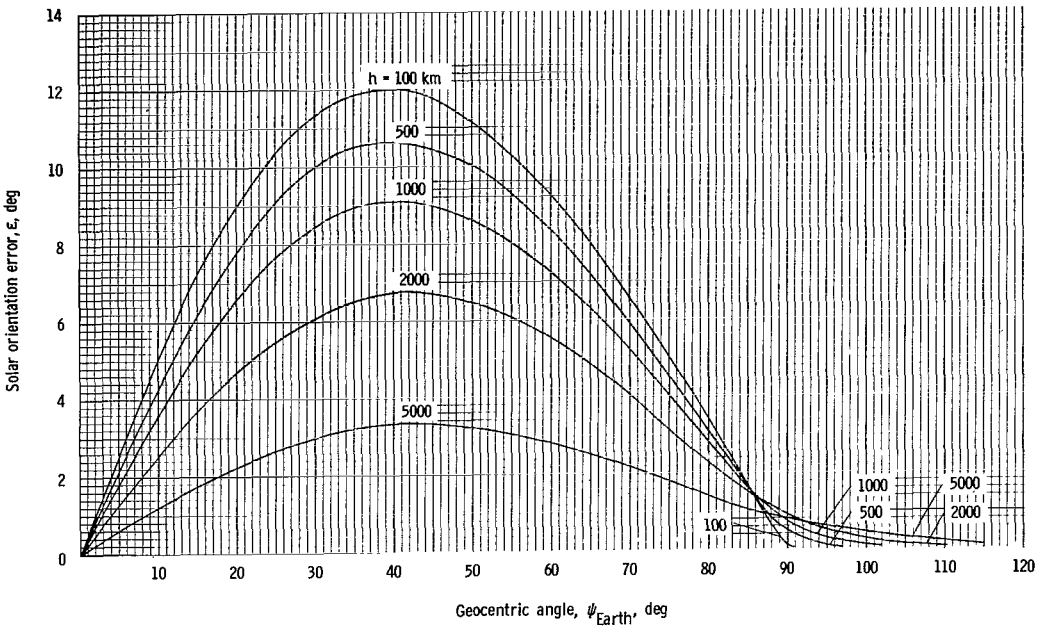

Figure 10.- Solar orientation error due to Earth albedo, a = 0.35.

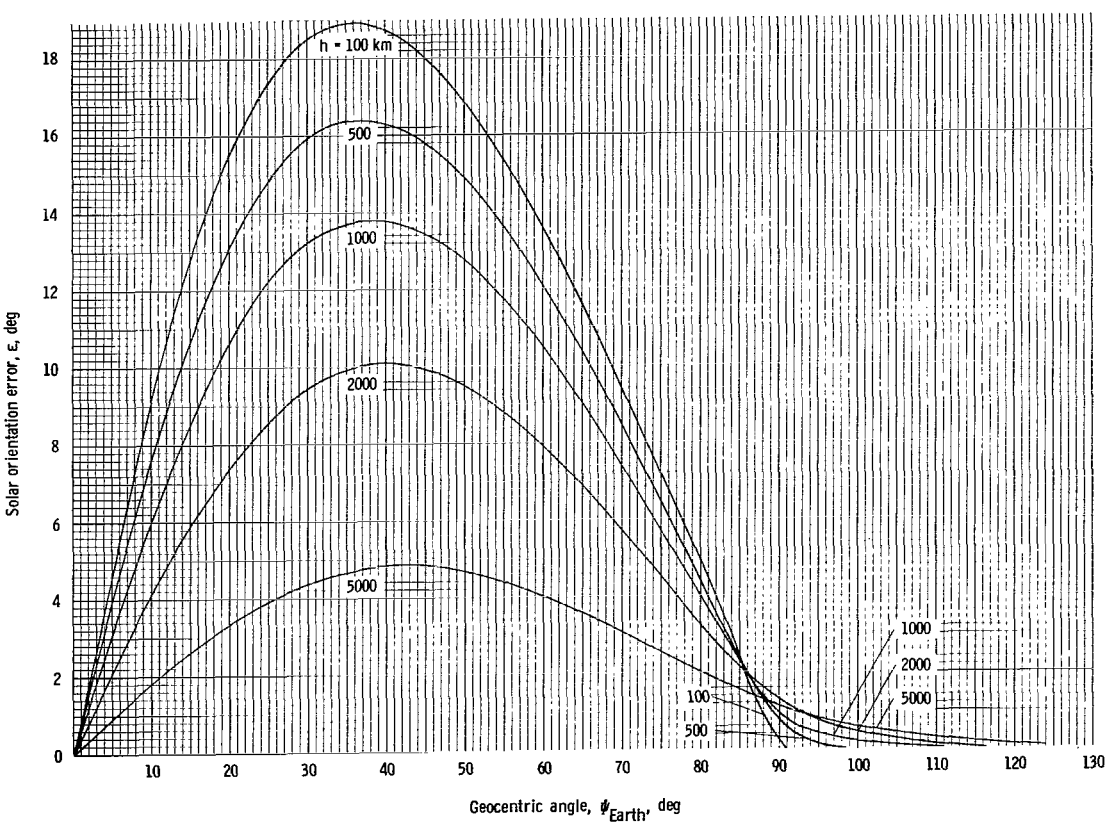

Figure 11.- Solar orientation error due to Earth albedo, a = 0.50.

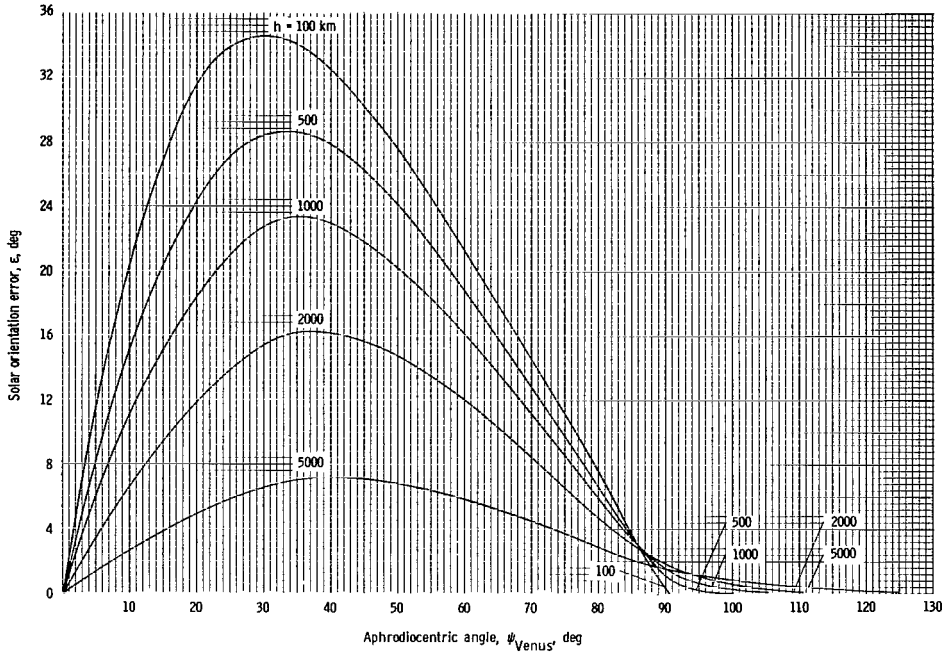

Figure 12.- Solar orientation error due to Venus albedo, a = 0.76.

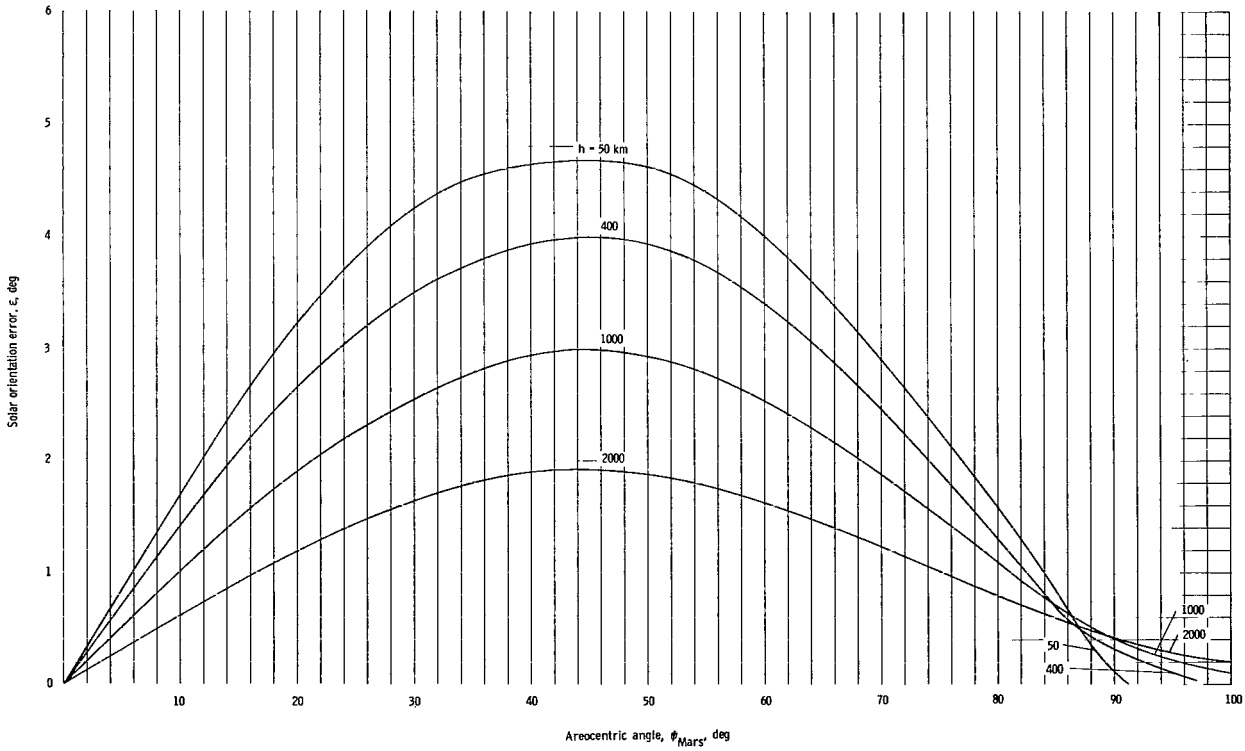

Figure 13.- Solar orientation error due to Mars albedo, a = 0.16.

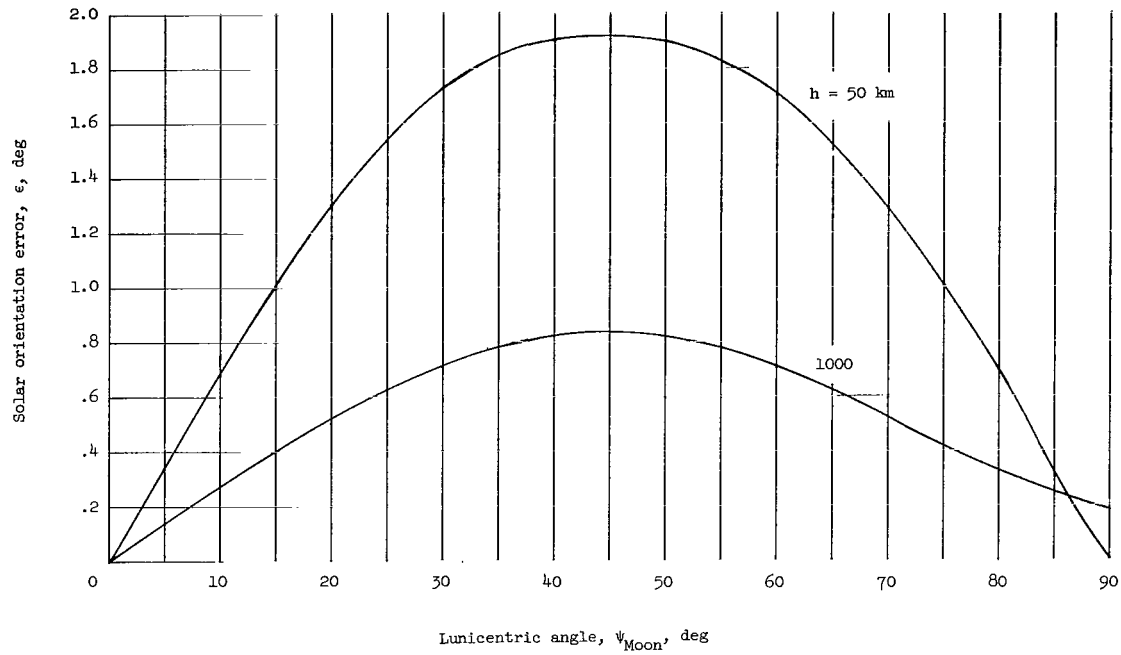

Figure 14.- Solar orientation error due to Moon albedo, a = 0.07.

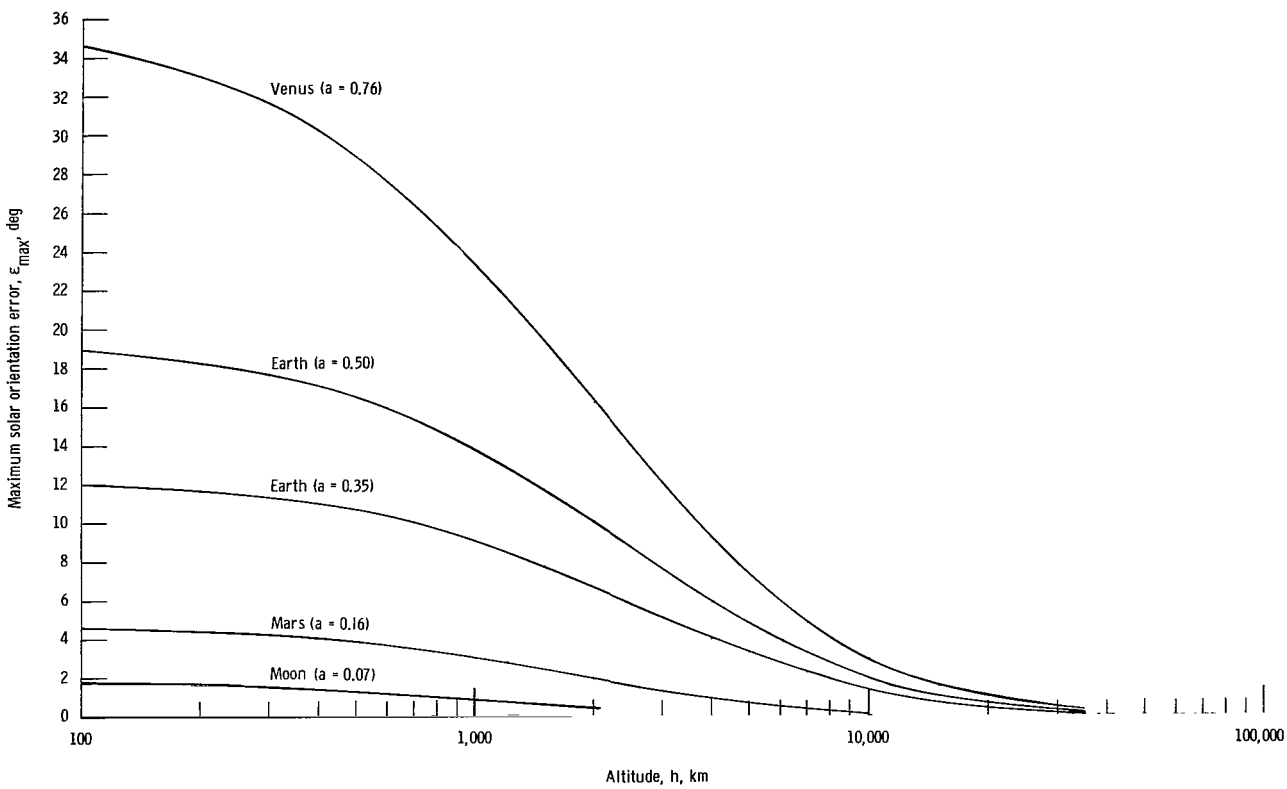

Figure 15.- Maximum solar orientation error due to planetary albedo.

COMMENTS ON ACCURACY

The departure of planetary bodies from diffuse reflectors is considered in reference 10. For planetocentric angles less than 90° the actual reflected radiance is less than that of a Lambert sphere, with the result that the solar orientation errors calculated herein are larger than the actual errors. However, it should be noted that, although specular reflection is not directly considered in this analysis, the albedo magnitudes indirectly compensate for the departure from diffuse reflection. (The Earth albedo of 0.70, measured by Tiros VII, was apparently due to specular reflection from polar caps and large bodies of water.) A primary source of inaccuracy is the inability to precisely specify the planetary albedos. When albedo magnitudes are known more accurately, the data generated herein can be updated by direct substitution of the albedo magnitudes into the existing analytical expressions. Consideration of the variation of albedo with latitude and season (when such information is available) will require a major change in the analytical expressions and will most probably result in a significant increase in complexity. The assumption of cylindrical planetary shadows introduces negligible error relative to the accuracy of the calculations – that is, for all cases considered, the solar orientation error decreases to less than 0.1° before the penumbra is encountered. Similarly, the assumption of spherical planetary bodies introduces negligible inaccuracy.

When investigating a specific application, more accurate results can be obtained by replacing the assumed sinusoidal coarse-sensor output characteristic with a mathematical model of the actual coarse-sensor output characteristic. The resulting increase in complexity depends on how accurately the sensor characteristic is described.

CONCLUDING REMARKS

The herein derived equation for the solar orientation error caused by planetary albedo is an exact expression (even though it has not been solved explicitly) only for the geometric aspects of the problem. The departure of planetary bodies from diffuse reflectors and the uncertainty of specified planetary albedos are primary sources of inaccuracy. The assumption of spherical planetary bodies with cylindrical shadows introduces negligible inaccuracy. The restriction of the pitch-plane orientation does not affect accuracy.

The assumption of a sinusoidal solar sensor output characteristic permits a straightforward computer solution to the analytical expressions. The relatively large albedos of Venus and Earth produce relatively large solar orientation errors whereas the relatively small albedos of Mars and the Moon produce relatively small solar orientation errors. The maximum solar orientation error at an altitude of 200 kilometers is 32.9° for Venus

(albedo of 0.76), 18.3° for Earth (albedo of 0.50), 4.4° for Mars (albedo of 0.16), and 1.7° for the Moon (albedo of 0.07). The maximum orientation errors occur between planetocentric angles of 30° and 45°. The solar orientation error decreases with increasing altitude.

The calculated solar orientation errors are presented as functions of altitude and planetocentric angle. These data permit the selection of an appropriate coarse-sensor to fine-sensor switching angle for solar orientation control systems and facilitate the interpretation of solar-referenced instrument and experiment data.

Langley Research Center,
National Aeronautics and Space Administration,
Langley Station, Hampton, Va., March 1, 1967,
125-19-03-09-23.

REFERENCES

1. Fontana, Anthony: A Photovoltaic Solar Sensor for Use in Spacecraft Orientation Control Systems. NASA TN D-3279, 1966.

2. Powers, Edward I.: Thermal Radiation to a Flat Surface Rotating About an Arbitrary Axis in an Elliptical Earth Orbit: Application to Spin-Stabilized Satellites. NASA TN D-2147, 1964.

3. Bannister, Tommy C.: Radiation Geometry Factor Between the Earth and a Satellite. NASA TN D-2750, 1965.

4. Cunningham, Fred G.: Earth Reflected Solar Radiation Incident Upon an Arbitrarily Oriented Spinning Flat Plate. NASA TN D-1842, 1963.

5. Gondolatsch, F.; and Kuiper, G. P.: Planets and Satellites. Landolt-Börnstein Numerical Data and Functional Relationships in Science and Technology, Group VI, Vol. I, H. H. Voigt, ed., Springer-Verlag, 1965, pp. 150-176.

6. Bandeen, W. R.; Halev, M.; and Strange, I.: A Radiation Climatology in the Visible and Infrared From the Tiros Meteorological Satellites. NASA TN D-2534, 1965.

7. Millard, John P.; and Neel, Carr B.: Albedo and Earth Radiation Deduced From Emissivity Sensors on the First Orbiting Solar Observatory. AIAA Paper No. 64-317, June-July 1964.

8. London, Julius: A Study of the Atmospheric Heat Balance. AFCRC-TR-57-287, ASTIA no. 117227, College Eng., New York Univ., July 1957.

9. Anon.: CE-3 Coarse Eye. Eng. Data Sheet BR-225, Ball Bros. Res. Corp., Nov. 1965.

10. Katzoff, S.: The Electromagnetic-Radiation Environment of a Satellite. Part I. Range of Thermal to X-Radiation. NASA TN D-1360, 1962.

TABLE I.- SOLAR ORIENTATION ERROR DUE TO EARTH ALBEDO OF 0.35

ψ_{Earth}, deg	ϵ, deg, at altitude of –																					
	100 km	200 km	300 km	400 km	500 km	600 km	700 km	800 km	900 km	1000 km	1500 km	2000 km	2500 km	3000 km	4000 km	5000 km	7000 km	10 000 km	15 000 km	20 000 km	25 000 km	35 000 km
0	0	0	0	0	0	0	0	0	0	0	0	0	0	0	0	0	0	0	0	0	0	0
5	2.6	2.5	2.4	2.3	2.2	2.1	2.1	2.0	1.9	1.8	1.5	1.3	1.1	1.0	.8	.6	.4	.3	.1	.1	.1	0
10	5.0	4.9	4.7	4.5	4.3	4.2	4.0	3.9	3.7	3.6	3.0	2.6	2.2	1.9	1.5	1.2	.8	.5	.3	.2	.1	.1
15	7.2	7.0	6.7	6.5	6.2	6.0	5.8	5.6	5.4	5.2	4.4	3.7	3.2	2.8	2.2	1.7	1.2	.7	.4	.2	.2	.1
20	9.0	8.7	8.4	8.1	7.8	7.6	7.3	7.0	6.8	6.6	5.5	4.7	4.1	3.5	2.8	2.3	1.5	.9	.5	.3	.2	.1
25	10.4	10.1	9.7	9.4	9.1	8.8	8.5	8.2	7.9	7.6	6.5	5.5	4.8	4.2	3.3	2.6	1.8	1.1	.6	.4	.3	.1
30	11.3	11.0	10.7	10.3	10.0	9.6	9.3	9.0	8.7	8.4	7.2	6.2	5.3	4.7	3.6	2.9	2.0	1.2	.7	.4	.3	.2
35	11.9	11.5	11.2	10.8	10.5	10.1	9.8	9.5	9.2	8.9	7.6	6.5	5.7	5.0	3.9	3.1	2.1	1.3	.7	.5	.3	.2
40	12.0	11.7	11.3	11.0	10.6	10.3	10.0	9.7	9.4	9.1	7.8	6.7	5.9	5.1	4.0	3.3	2.2	1.4	.8	.5	.3	.2
45	11.7	11.4	11.1	10.8	10.4	10.1	9.8	9.5	9.2	9.0	7.7	6.7	5.8	5.1	4.1	3.3	2.3	1.4	.8	.5	.3	.2
50	11.2	10.9	10.6	10.3	10.0	9.7	9.4	9.1	8.9	8.6	7.4	6.5	5.7	5.0	3.9	3.2	2.2	1.4	.8	.5	.3	.2
55	10.3	10.1	9.8	9.5	9.3	9.0	8.7	8.5	8.2	8.0	6.9	6.0	5.3	4.7	3.7	3.0	2.1	1.3	.8	.5	.3	.2
60	9.3	9.0	8.8	8.6	8.3	8.1	7.9	7.6	7.4	7.2	6.3	5.5	4.8	4.3	3.4	2.8	2.0	1.3	.7	.5	.3	.2
65	8.0	7.8	7.6	7.4	7.2	7.0	6.8	6.6	6.4	6.3	5.5	4.8	4.2	3.8	3.0	2.5	1.8	1.1	.7	.4	.3	.2
70	6.6	6.4	6.3	6.1	5.9	5.8	5.6	5.5	5.3	5.2	4.5	4.0	3.5	3.2	2.6	2.1	1.5	1.0	.6	.4	.3	.2
75	5.0	4.9	4.8	4.7	4.5	4.4	4.3	4.2	4.1	4.0	3.5	3.1	2.8	2.5	2.1	1.8	1.3	.9	.5	.3	.2	.1
80	3.4	3.3	3.2	3.2	3.1	3.0	2.9	2.9	2.8	2.8	2.5	2.3	2.1	1.9	1.6	1.4	1.1	.7	.4	.3	.2	.1
85	1.7	1.7	1.7	1.6	1.6	1.6	1.6	1.6	1.6	1.6	1.6	1.5	1.4	1.3	1.2	1.1	.8	.6	.4	.3	.2	.1
90	.1	.2	.3	.4	.5	.5	.6	.6	.7	.7	.8	.9	.9	.9	.8	.8	.6	.5	.3	.2	.2	.1
95	0	0	0	0.1	0.1	.1	.2	.2	.3	.3	.4	.5	.6	.6	.6	.6	.5	.4	.2	.2	.1	.1
100	0	0	0	0	0	0	.1	.1	.1	.1	.2	.3	.3	.4	.4	.4	.4	.3	.2	.1	.1	.1
105			0	0	0	0	0	0	0	0	.1	.1	.2	.2	.2	.3	.2	.2	.1	.1	.1	.1
110					0	0	0	0	0	0	0	.1	.1	.1	.2	.2	.1	.1	.1	.1	.1	0
115							0	0	0	0	0	0	0	.1	.1	.1	.1	.1	.1	.1	0	0
120										0	0	0	0	0	0	0	.1	.1	.1	0	0	0
125											0	0	0	0	0	0	0	0	0	0	0	0
130												0	0	0	0	0	0	0	0	0	0	0
135														0	0	0	0	0	0	0	0	0
140															0	0	0	0	0	0	0	0
145																0	0	0	0	0	0	0
150																	0	0	0	0	0	0
155																		0	0	0	0	0
160																			0	0	0	0
165																				0	0	0
170																						0

TABLE II.- SOLAR ORIENTATION ERROR DUE TO EARTH ALBEDO OF 0.50

ψ_{Earth}, deg	ϵ, deg, at altitude of –																						
	100 km	200 km	300 km	400 km	500 km	600 km	700 km	800 km	900 km	1000 km	1500 km	2000 km	2500 km	3000 km	4000 km	5000 km	7000 km	10 000 km	15 000 km	20 000 km	25 000 km	35 000 km
0	0	0	0	0	0	0	0	0	0	0	0	0	0	0	0	0	0	0	0	0	0	0
5	4.7	4.5	4.3	4.1	3.9	3.7	3.5	3.4	3.2	3.1	2.5	2.1	1.8	1.5	1.1	.9	.6	.4	.2	.1	.1	0
10	9.0	8.6	8.2	7.9	7.5	7.2	6.8	6.5	6.3	6.0	4.9	4.1	3.4	3.0	2.2	1.8	1.2	.7	.4	.2	.2	.1
15	12.7	12.1	11.6	11.1	10.6	10.1	9.7	9.3	8.9	8.5	7.0	5.9	5.0	4.3	3.3	2.6	1.7	1.1	.6	.4	.2	.1
20	15.5	14.9	14.2	13.6	13.1	12.5	12.0	11.5	11.1	10.6	8.8	7.4	6.3	5.4	4.1	3.3	2.2	1.3	.7	.5	.3	.2
25	17.4	16.8	16.1	15.5	14.8	14.3	13.7	13.2	12.7	12.2	10.1	8.6	7.3	6.3	4.9	3.9	2.6	1.6	.9	.5	.4	.2
30	18.5	17.9	17.2	16.6	15.9	15.3	14.8	14.2	13.7	13.2	11.1	9.4	8.1	7.0	5.4	4.3	2.9	1.8	1.0	.6	.4	.2
35	18.9	18.3	17.7	17.0	16.4	15.8	15.3	14.7	14.2	13.7	11.6	9.9	8.5	7.4	5.8	4.6	3.1	1.9	1.1	.7	.5	.3
40	18.7	18.1	17.5	16.9	16.3	15.8	15.3	14.8	14.3	13.8	11.7	10.1	8.7	7.6	5.9	4.8	3.2	2.0	1.1	.7	.5	.3
45	18.0	17.4	16.9	16.3	15.8	15.3	14.8	14.3	13.9	13.4	11.5	9.9	8.6	7.6	5.9	4.8	3.3	2.1	1.1	.7	.5	.3
50	16.8	16.3	15.9	15.4	14.9	14.4	14.0	13.6	13.2	12.7	11.0	9.5	8.3	7.3	5.7	4.6	3.2	2.0	1.1	.7	.5	.3
55	15.3	14.9	14.5	14.1	13.6	13.2	12.8	12.5	12.1	11.7	10.1	8.8	7.7	6.8	5.4	4.4	3.0	1.9	1.1	.7	.5	.3
60	13.6	13.2	12.9	12.5	12.1	11.8	11.4	11.1	10.8	10.5	9.1	7.9	7.0	6.2	4.9	4.0	2.8	1.8	1.0	.7	.5	.3
65	11.6	11.3	11.0	10.7	10.4	10.1	9.8	9.5	9.3	9.0	7.9	6.9	6.1	5.4	4.3	3.6	2.5	1.6	.9	.6	.4	.2
70	9.5	9.3	9.0	8.8	8.5	8.3	8.0	7.8	7.6	7.4	6.5	5.7	5.1	4.5	3.7	3.1	2.2	1.5	.8	.6	.4	.2
75	7.2	7.0	6.9	6.7	6.5	6.3	6.2	6.0	5.8	5.7	5.0	4.5	4.0	3.6	3.0	2.5	1.9	1.3	.7	.5	.3	.2
80	4.9	4.7	4.6	4.5	4.4	4.3	4.2	4.1	4.0	3.9	3.5	3.2	3.0	2.7	2.3	2.0	1.5	1.0	.6	.4	.3	.2
85	2.4	2.4	2.4	2.3	2.3	2.3	2.3	2.3	2.3	2.3	2.2	2.1	2.0	1.8	1.7	1.5	1.2	.8	.5	.4	.3	.2
90	.2	.3	.5	.6	.7	.8	.8	.9	.9	.9	1.2	1.3	1.3	1.3	1.2	1.1	.9	.7	.4	.3	.2	.1
95	0	0	.1	.1	.1	.2	.3	.3	.4	.4	.6	.7	.8	.8	.8	.8	.7	.5	.4	.2	.2	.1
100	0	0	0	0	0	.1	.1	.1	.1	.2	.3	.4	.5	.5	.6	.6	.5	.4	.3	.2	.1	.1
105			0	0	0	0	0	0	0	0	.1	.2	.2	.3	.3	.4	.4	.3	.2	.2	.1	.1
110					0	0	0	0	0	0	0	.1	.1	.2	.2	.2	.2	.2	.2	.1	.1	.1
115							0	0	0	0	0	0	.1	.1	.1	.1	.2	.1	.1	.1	.1	0
120										0	0	0	0	0	.1	.1	.1	.1	.1	.1	0	0
125											0	0	0	0	0	0	0	.1	.1	0	0	0
130												0	0	0	0	0	0	0	0	0	0	0
135														0	0	0	0	0	0	0	0	0
140															0	0	0	0	0	0	0	0
145																0	0	0	0	0	0	0
150																	0	0	0	0	0	0
155																		0	0	0	0	0
160																			0	0	0	0
165																				0	0	0
170																						0

TABLE III.- SOLAR ORIENTATION ERROR DUE TO VENUS ALBEDO OF 0.76

ψ_{Venus}, deg	ϵ, deg, at altitude of –																					
	100 km	200 km	300 km	400 km	500 km	600 km	700 km	800 km	900 km	1000 km	1500 km	2000 km	2500 km	3000 km	4000 km	5000 km	7000 km	10 000 km	15 000 km	20 000 km	25 000 km	35 000 km
0	0	0	0	0	0	0	0	0	0	0	0	0	0	0	0	0	0	0	0	0	0	0
5	11.3	10.4	9.6	8.8	8.2	7.6	7.1	6.6	6.2	5.9	4.5	3.5	2.9	2.4	1.7	1.3	.9	.5	.3	.2	.1	.1
10	20.0	18.5	17.1	15.9	14.8	13.8	12.9	12.1	11.4	10.8	8.3	6.6	5.4	4.5	3.3	2.5	1.6	1.0	.5	.3	.2	.1
15	26.9	24.9	23.2	21.6	20.2	18.9	17.8	16.7	15.8	15.0	11.6	9.3	7.7	6.5	4.8	3.7	2.4	1.5	.8	.5	.3	.2
20	31.5	29.5	27.6	25.9	24.3	22.9	21.6	20.5	19.4	18.4	14.5	11.8	9.8	8.3	6.2	4.8	3.2	2.0	1.1	.6	.4	.2
25	33.9	32.0	30.3	28.6	27.1	25.7	24.4	23.2	22.1	21.0	16.8	13.8	11.6	9.9	7.5	5.9	3.9	2.3	1.2	.8	.5	.3
30	34.6	32.9	31.3	29.8	28.4	27.1	25.9	24.8	23.7	22.7	18.5	15.4	13.0	11.2	8.5	6.6	4.3	2.6	1.4	.9	.6	.3
35	33.9	32.5	31.1	29.8	28.6	27.5	26.4	25.3	24.3	23.4	19.4	16.2	13.7	11.8	8.9	7.0	4.6	2.8	1.5	.9	.6	.4
40	32.4	31.2	30.0	28.9	27.9	26.8	25.7	24.8	23.8	22.9	19.1	16.1	13.8	11.9	9.1	7.2	4.8	3.0	1.6	1.0	.7	.4
45	30.2	29.2	28.2	27.2	26.2	25.2	24.3	23.4	22.6	21.8	18.3	15.6	13.4	11.6	9.0	7.1	4.8	3.0	1.6	1.0	.7	.4
50	27.6	26.8	25.8	24.9	24.0	23.2	22.4	21.6	20.9	20.2	17.2	14.7	12.7	11.1	8.6	6.9	4.7	2.9	1.6	1.0	.7	.4
55	24.7	23.9	23.1	22.3	21.6	20.8	20.2	19.5	18.9	18.3	15.6	13.5	11.7	10.3	8.1	6.5	4.4	2.8	1.5	1.0	.7	.4
60	21.5	20.8	20.1	19.5	18.9	18.3	17.7	17.1	16.6	16.1	13.8	12.0	10.5	9.2	7.3	5.9	4.1	2.6	1.5	.9	.6	.4
65	18.1	17.5	17.0	16.5	16.0	15.5	15.0	14.5	14.1	13.7	11.9	10.3	9.1	8.0	6.4	5.2	3.7	2.4	1.3	.9	.6	.3
70	14.6	14.2	13.8	13.3	12.9	12.5	12.2	11.8	11.5	11.1	9.7	8.5	7.5	6.7	5.4	4.5	3.2	2.1	1.2	.8	.6	.3
75	11.0	10.7	10.4	10.1	9.8	9.5	9.2	9.0	8.7	8.5	7.5	6.6	5.9	5.3	4.4	3.7	2.7	1.8	1.1	.7	.5	.3
80	7.4	7.2	7.0	6.8	6.7	6.4	6.3	6.1	6.0	5.9	5.3	4.8	4.4	4.0	3.4	2.9	2.2	1.5	.9	.6	.4	.3
85	3.7	3.6	3.6	3.5	3.5	3.5	3.4	3.4	3.4	3.4	3.3	3.2	3.0	2.9	2.5	2.2	1.7	1.2	.8	.5	.4	.2
90	.3	.5	.7	.9	1.1	1.2	1.3	1.4	1.5	1.6	1.8	1.9	2.0	1.9	1.8	1.6	1.3	1.0	.6	.4	.3	.2
95	0	0	.1	.2	.2	.3	.4	.5	.6	.7	1.0	1.1	1.2	1.3	1.3	1.2	1.0	.8	.5	.4	.3	.2
100	0	0	0	0	.1	.1	.1	.2	.2	.2	.5	.6	.7	.8	.9	.8	.8	.6	.4	.3	.2	.1
105			0	0	0	0	0	0	.1	.1	.2	.3	.4	.5	.5	.6	.5	.4	.3	.2	.2	.1
110				0	0	0	0	0	0	0	.1	.1	.2	.2	.3	.4	.4	.3	.2	.2	.1	.1
115							0	0	0	0	0	0	.1	.1	.2	.2	.2	.2	.2	.1	.1	.1
120										0	0	0	0	0	.1	.1	.1	.1	.1	.1	.1	0
125											0	0	0	0	0	.1	.1	.1	.1	.1	0	0
130												0	0	0	0	0	0	0	0	0	0	0
135														0	0	0	0	0	0	0	0	0
140															0	0	0	0	0	0	0	0
145																0	0	0	0	0	0	0
150																	0	0	0	0	0	0
155																		0	0	0	0	0
160																			0	0	0	0
165																				0	0	0
170																						0

TABLE IV.- SOLAR ORIENTATION ERROR

DUE TO MARS ALBEDO OF 0.16

ψ_{Mars}, deg	ϵ, deg, at altitude of –													
	50 km	200 km	400 km	600 km	800 km	1000 km	1500 km	2000 km	2500 km	3000 km	4000 km	5000 km	7000 km	10 000 km
0	0	0	0	0	0	0	0	0	0	0	0	0	0	0
5	.9	.8	.7	.7	.6	.5	.4	.3	.3	.2	.2	.1	.1	0
10	1.7	1.6	1.4	1.3	1.1	1.0	.8	.6	.5	.4	.3	.2	.1	.1
15	2.5	2.3	2.1	1.8	1.6	1.5	1.1	.9	.7	.6	.4	.3	.2	.1
20	3.2	2.9	2.6	2.3	2.1	1.9	1.5	1.2	.9	.8	.6	.4	.3	.2
25	3.7	3.4	3.1	2.8	2.5	2.2	1.7	1.4	1.1	1.0	.7	.5	.3	.2
30	4.2	3.9	3.5	3.1	2.8	2.5	2.0	1.6	1.3	1.1	.8	.6	.4	.2
35	4.5	4.2	3.7	3.4	3.0	2.7	2.2	1.8	1.5	1.2	.9	.7	.4	.2
40	4.6	4.3	3.9	3.5	3.2	2.9	2.3	1.9	1.5	1.3	.9	.7	.4	.2
45	4.7	4.4	4.0	3.6	3.3	3.0	2.4	1.9	1.5	1.3	.9	.7	.4	.2
50	4.6	4.3	3.9	3.6	3.2	2.9	2.3	1.9	1.5	1.3	.9	.7	.4	.2
55	4.4	4.1	3.7	3.4	3.1	2.8	2.2	1.8	1.4	1.2	.9	.7	.4	.2
60	4.0	3.8	3.4	3.1	2.8	2.5	2.0	1.6	1.3	1.1	.8	.6	.4	.2
65	3.5	3.3	3.0	2.7	2.5	2.2	1.8	1.4	1.2	1.0	.7	.6	.4	.2
70	2.9	2.8	2.5	2.3	2.1	1.9	1.5	1.2	1.0	.9	.6	.5	.3	.2
75	2.3	2.1	1.9	1.8	1.6	1.5	1.2	1.0	.8	.7	.5	.4	.3	.2
80	1.6	1.5	1.3	1.2	1.1	1.1	.9	.8	.7	.6	.4	.4	.2	.1
85	.8	.8	.7	.7	.7	.7	.6	.6	.5	.4	.4	.3	.2	.1
90	.1	.2	.3	.3	.4	.4	.4	.4	.4	.3	.3	.2	.2	.1
95	0	0	.1	.1	.2	.2	.3	.3	.3	.2	.2	.2	.1	.1
100		0	0	.1	.1	.1	.2	.2	.2	.2	.2	.1	.1	.1
105		0	0	0	0	.1	.1	.1	.1	.1	.1	.1	.1	.1
110			0	0	0	0	0	.1	.1	.1	.1	.1	.1	0
115			0	0	0	0	0	0	0	0	0	0	0	0
120				0	0	0	0	0	0	0	0	0	0	0
125					0	0	0	0	0	0	0	0	0	0
130							0	0	0	0	0	0	0	0
135							0	0	0	0	0	0	0	0
140								0	0	0	0	0	0	0
145										0	0	0	0	0
150											0	0	0	0
155												0	0	0
160													0	0
165														0

TABLE V.- SOLAR ORIENTATION ERROR

DUE TO MOON ALBEDO OF 0.07

ψ_{Moon}, deg	ϵ, deg, at altitude of –				
	50 km	200 km	500 km	1000 km	2000 km
0	0	0	0	0	0
5	.4	.3	.2	.1	.1
10	.7	.6	.4	.3	.1
15	1.0	.8	.6	.4	.2
20	1.3	1.1	.8	.5	.3
25	1.5	1.3	.9	.6	.3
30	1.7	1.4	1.1	.7	.4
35	1.8	1.6	1.2	.8	.4
40	1.9	1.7	1.2	.8	.4
45	1.9	1.7	1.3	.8	.4
50	1.9	1.7	1.3	.8	.4
55	1.8	1.6	1.2	.8	.4
60	1.7	1.5	1.1	.7	.4
65	1.5	1.3	1.0	.6	.3
70	1.3	1.1	.8	.5	.3
75	1.0	.9	.7	.4	.2
80	.7	.6	.5	.3	.2
85	.3	.3	.3	.3	.2
90	0	.1	.2	.2	.1
95	0	0	.1	.1	.1
100	0	0	0	.1	.1
105		0	0	0	0
110		0	0	0	0
115		0	0	0	0
120			0	0	0
125			0	0	0
130				0	0
135				0	0
140				0	0
145					0
150					0

"The aeronautical and space activities of the United States shall be conducted so as to contribute . . . to the expansion of human knowledge of phenomena in the atmosphere and space. The Administration shall provide for the widest practicable and appropriate dissemination of information concerning its activities and the results thereof."

—NATIONAL AERONAUTICS AND SPACE ACT OF 1958

NASA SCIENTIFIC AND TECHNICAL PUBLICATIONS

TECHNICAL REPORTS: Scientific and technical information considered important, complete, and a lasting contribution to existing knowledge.

TECHNICAL NOTES: Information less broad in scope but nevertheless of importance as a contribution to existing knowledge.

TECHNICAL MEMORANDUMS: Information receiving limited distribution because of preliminary data, security classification, or other reasons.

CONTRACTOR REPORTS: Scientific and technical information generated under a NASA contract or grant and considered an important contribution to existing knowledge.

TECHNICAL TRANSLATIONS: Information published in a foreign language considered to merit NASA distribution in English.

SPECIAL PUBLICATIONS: Information derived from or of value to NASA activities. Publications include conference proceedings, monographs, data compilations, handbooks, sourcebooks, and special bibliographies.

TECHNOLOGY UTILIZATION PUBLICATIONS: Information on technology used by NASA that may be of particular interest in commercial and other non-aerospace applications. Publications include Tech Briefs, Technology Utilization Reports and Notes, and Technology Surveys.

Details on the availability of these publications may be obtained from:

SCIENTIFIC AND TECHNICAL INFORMATION DIVISION

NATIONAL AERONAUTICS AND SPACE ADMINISTRATION

Washington, D.C. 20546